 doi:10.20944/preprints202104.0314.v1

Article

Interface Joint Strength Between SS316L Wrought Substrate and Powder Bed Fusion Built Parts

Jason M. Weaver [1]*, John R. Linn [1], Michael P. Miles [1]

[1] Brigham Young University, Provo Utah, USA 84602
* Correspondence: jasonweaver@byu.edu

Abstract: Metal powder bed fusion (PBF) additive manufacturing (AM) builds metal parts layer by layer upon a substrate material. The strength of this interface between substrate and printed material is important to characterize, especially in applications where the substrate is retained and included in the finished part. This paper studied the tensile and torsional strengths of wrought and additively manufactured (through PBF) SS316L and compared them to specimens composed of half wrought material and half PBF material. The PBF specimens consistently exhibited higher strength and lower ductility than the wrought specimens. The hybrid PBF/wrought specimens performed similarly to the wrought material. In no specimens did any failure appear to occur at or near the interface between wrought substrate and PBF material. In addition, most of the deformation in the PBF/wrought specimens appeared to be limited to the wrought portion of the specimens. These results are consistent with microscopy showing smaller grain size in the PBF material, which often leads to increased strength in SS316L due to the Hall-Petch relationship.

Keywords: powder bed fusion; additive manufacturing; ss316l; interface strength

1. Introduction

Additive manufacturing (AM) of metals can currently be accomplished through several different methods. The two most common technologies in industrial settings are powder bed fusion (PBF) and directed energy deposition (DED). In PBF processes, metal powder or wire is spread evenly over a flat surface and selectively welded or sintered together by a laser, electron beam, or other energy source [1]. In DED processes, metal particles are fed into a melt pool on a work surface and simultaneously welded together, again by a laser, electron beam, or other energy source [2]. In both PBF and DED, the fused metal particles build upon an existing substrate material. Often, the desired part is usually distinct from the substrate and is cut off in post-processing. However, in certain applications, the substrate remains an integral part of the finished product [3].

DED is often the AM process of choice for applications where the substrate is an existing part, as it can more easily build off non-horizontal or complex surfaces [4]. PBF processes are currently more generally available in industry and often have better accuracy and surface finish, but any substrate surface being printed on must be planar and secured horizontally in the powder bed [5]. Because of this limitation, the use of PBF to print onto existing structures that are retained in the final part has not been as extensively studied.

There are several scenarios where the ability to print onto existing structures would be beneficial. One application of interest is the capability to build new features on a part manufactured through other means. Many products (such as aircraft engine turbines, oil drill bits, and friction stir welding tools) consist of features with very complex geometries attached to a central body with simple geometry (like a cylindrical shaft). Using AM to print the complex features can save on machining costs and material waste, while also allowing greater design flexibility. However, also printing the simple shaft or hub would be needlessly expensive and inefficient. The AM features could be printed separately, then attached via welding or mechanical fasteners, but this is often undesirable due to reduced strength and added assembly time and complexity. If the complex features can be printed

Preprints (www.preprints.org) | NOT PEER-REVIEWED | Posted: 12 April 2021 doi:10.20944/preprints202104.0314.v1

directly onto a conventionally manufactured shaft or hub, a superior product and overall manufacturing process is possible.

Another similar application is the remanufacturing or repair of high-wear parts that would be expensive to replace [6]. For example, if a single turbine blade in an aircraft engine becomes damaged and cannot be repaired, either the blade must be removed and replaced, or even worse, the entire turbine must be replaced. If instead, the damage can be repaired by filling the damaged area using metal AM processes and then machining the new material to the required tolerances, the original part can still be used [7].

These applications are becoming more common in DED processes. For PBF to be considered for use in these applications as well, the material characteristics at the interface between the original substrate material and the new AM material must be understood. Ideally, the characteristics at the interface should be identical to or better than the characteristics of the original material and printed material. If the interface does exhibit suboptimal characteristics, these should be compared to those of the original material and printed material to determine if the proposed processes are acceptable solutions for building hybrid AM/conventional parts.

This paper will characterize the mechanical properties at or near the interface of test specimens built from SS316L stainless steel, using a PBF AM process.

2. Materials and Methods

A summary of the number and types of prepared specimens and completed tests is shown in Table 1. Specimens of wrought SS316L and AM-printed SS316L were compared to hybrid specimens of half-wrought, half-AM SS316L to evaluate the interface bond quality of the AM/wrought specimens. A 400W EOS M280 PBF-laser system was used to manufacture the AM and hybrid AM/wrought specimens from SS316L. Stock settings for the material were used on the machine.

Blocks of wrought material and blocks produced by PBF were machined into test specimens for evaluating tension and torsion responses, following ASTM E8 specifications [8]. The dimensions of the machined test specimens are shown in Figure 1 and Figure 2, along with photographs of sample PBF/wrought specimens.

Table 1. Summary of test specimens.

	SS316L specimens		
	Wrought	PBF	PBF/Wrought
Tension	3	3	3
Torsion	2 [1]	3	3
Microscopy	-	-	1

[1] One additional SS316L wrought torsion specimen was not included due to testing irregularities.

Preprints (www.preprints.org) | NOT PEER-REVIEWED | Posted: 12 April 2021 doi:10.20944/preprints202104.0314.v1

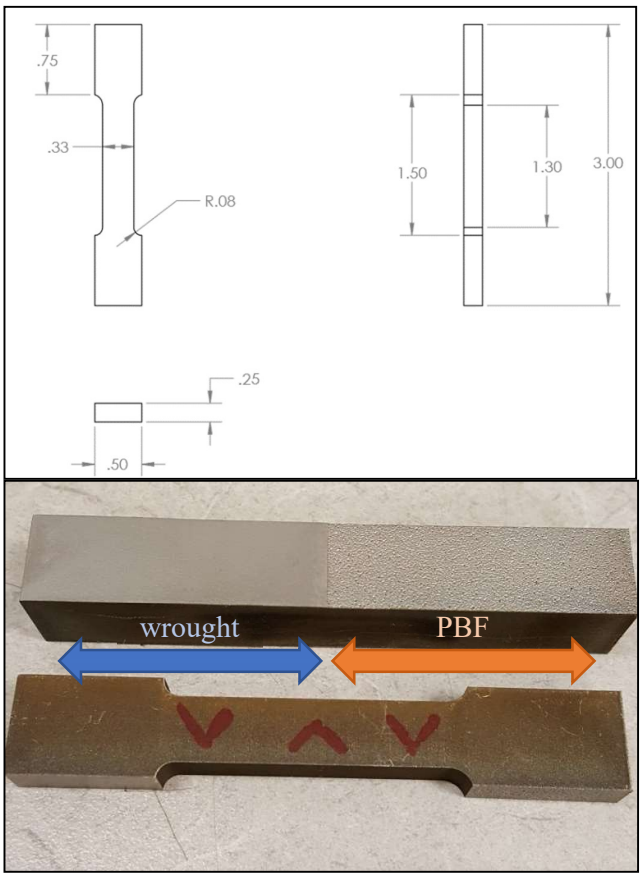

Figure 1. Tensile specimen design.

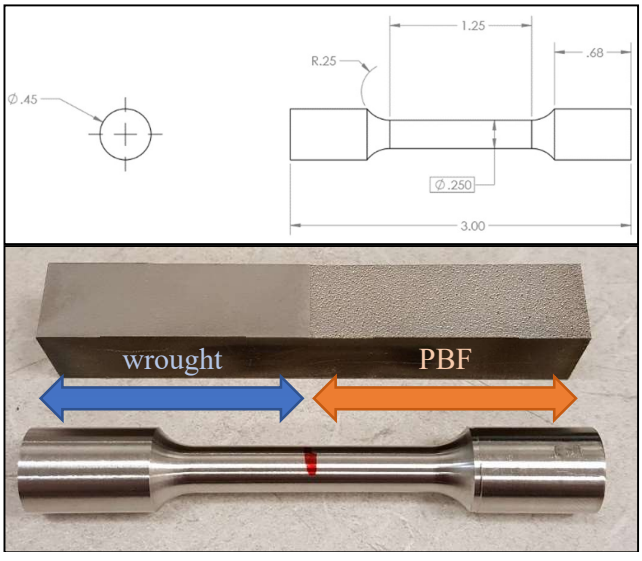

Figure 2. Torsion specimen design.

Tensile testing was performed on an Instron Model 1381 frame, with 8800 controller. Testing was conducted using the following parameters:

- Pull rate of 2 in/min
- Data acquisition at 10 Hz
- Measured: elongation (in) vs tensile load (lb)

Preprints (www.preprints.org) | NOT PEER-REVIEWED | Posted: 12 April 2021 doi:10.20944/preprints202104.0314.v1

The measured elongations and tensile loads were converted to strain and tensile stress in SI units using the standard formulas.

Torsion testing was performed on the same Instron machine, using the following parameters:

- Rotation rate of 6 deg/min
- Rotation range of 90 deg
- Data acquisition at 10 Hz
- Measured: rotation (deg) vs torque load (in-lb)

The measured torque load and rotation were converted to maximum shear stress in SI units (using the formula $\tau = T\,r\,/\,J$, where τ is maximum shear stress, T is measured torque load, r is the radius at the location of interest, and J is the polar moment of inertia for a cylinder, $\pi\,r^4\,/\,2$) and rotation per unit length of the narrow section (in rad/m).

A specimen was also prepared for visual analysis via microscopy. The microscopy specimen was cut on a wire EDM with the boundary between the PBF and wrought material centered on the face. The specimen was placed in an epoxy puck, ground progressively to 1200-grit sandpaper, polished with diamond paste and alumina, and then etched using Carpenter 300 Series stainless steel etchant. The specimen was also prepared for electron backscatter diffraction (EBSD) by the polishing routine described above, followed by an electropolish in perchloric acid-methanol solution and polish with colloidal silica. The etched microscopy specimen is shown in Figure 3. The finished microscopy specimen was viewed under a microscope at 32X and 63X magnification.

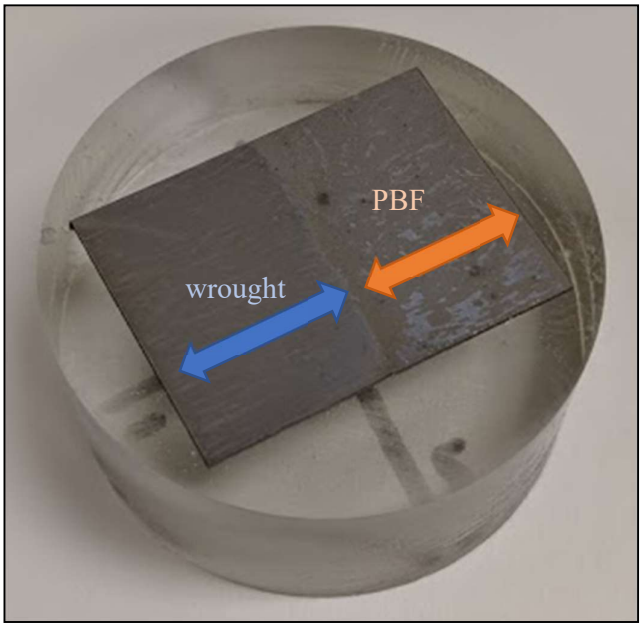

Figure 3. Etched PBF/wrought SS316L microscopy specimen.

3. Results

The tensile testing results are shown below in Figure 4, comparing the wrought and PBF/wrought specimens, where each curve represents an average of three specimens in each case. Note that stress and strain measured are engineering (nominal) stress and strain. The wrought and PBF/wrought specimens performed similarly under elastic deformation, while the PBF specimens exhibited a much higher yield strength and ultimate tensile strength. Both the monolithic PBF and the PBF/wrought specimens failed at lower strain than the wrought SS316L. After initial yielding, the PBF failed at the lowest strain, followed by the PBF/wrought specimens and then the wrought specimens. Necking and failure in PBF/wrought specimens occurred within the wrought material in each case.

Preprints (www.preprints.org) | NOT PEER-REVIEWED | Posted: 12 April 2021 doi:10.20944/preprints202104.0314.v1

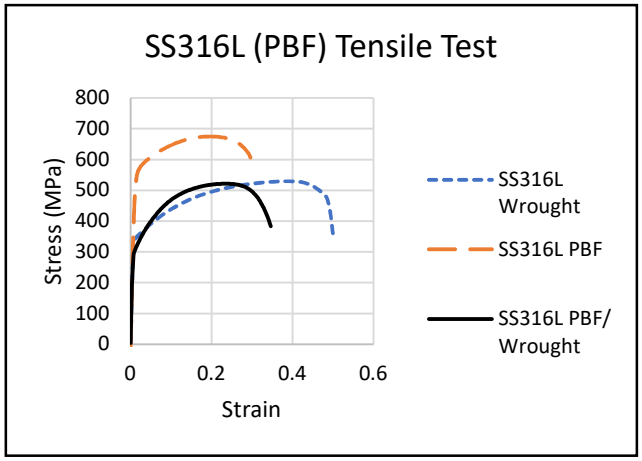

Figure 4. Average tensile test stress/strain.

Table 2 shows the average yield strength (σ_y) and ultimate tensile strength (σ_u) for the wrought, PBF, and PBF/wrought specimens. Table 3 shows the statistical analysis (α=0.05), which found significant difference in σ_y and σ_u between the PBF specimens and the two others.

Table 2. Measured tensile properties.

		Wrought	PBF	PBF/Wrought
σ_y	Mean	320 MPa	550 MPa	300 MPa
	StdDev	9.7 MPa	2.4 MPa	51 MPa
σ_u	Mean	530 MPa	680 MPa	520 MPa
	StdDev	1.0 MPa	2.6 MPa	30 MPa

Table 3. Statistical analysis of tensile samples.

	Comparison	Statistical test (α=0.05)	Different? (p ≤ 5.0E-2)
σ_y	Among group	ANOVA	**Yes** (p = 4.7E-4)
	Wrought vs PBF	t-test (equal variance)	**Yes** (p = 3.1E-5)
	Wrought vs PBF/Wrought	t-test (equal variance)	**No** (p = 5.4E-1)
	PBF vs PBF/Wrought	t-test (uneq. variance)	**Yes** (p = 1.4E-2)
σ_U	Among group	ANOVA	**Yes** (p = 3.1E-4)
	Wrought vs PBF	t-test (equal. variance)	**Yes** (p = 6.2E-6)
	Wrought vs PBF/Wrought	t-test (uneq. variance)	**No** (p = 6.3E-1)
	PBF vs PBF/Wrought	t-test (uneq. variance)	**Yes** (p = 1.2E-2)

Preprints (www.preprints.org) | NOT PEER-REVIEWED | Posted: 12 April 2021 doi:10.20944/preprints202104.0314.v1

3.2. Torsion Testing

The results of a torsion test are shown below in Figure 5, where deformation is concentrated in the wrought portion of the specimen. This was the same tendency seen in the tensile specimens.

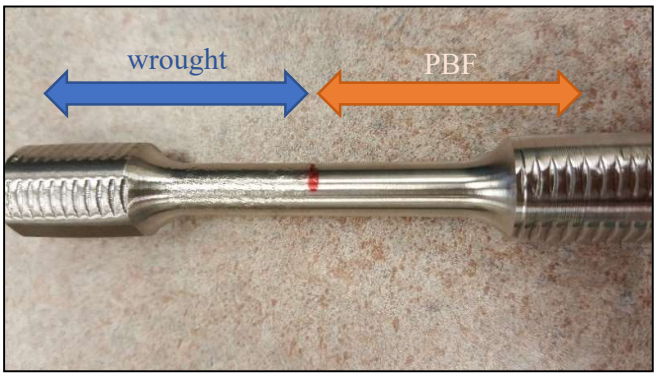

Figure 5. SS316L (PBF/wrought) torsion specimen post-failure.

Figure 6 shows the average stress profiles of SS316L in torsion for the 2 wrought, 3 PBF, and 3 PBF/wrought specimens. The wrought and PBF/wrought specimens performed similarly, while the PBF specimens exhibited a much higher τ_y. Table 4 shows the average torsional yield strength (τ_y) and shear modulus (G) for the wrought, PBF, and PBF/wrought specimens.

Preprints (www.preprints.org) | NOT PEER-REVIEWED | Posted: 12 April 2021 doi:10.20944/preprints202104.0314.v1

Table 5 shows the shows the statistical analysis (α=0.05), which found the difference in τ_y in PBF specimens from the other two groups to be significant. The differences in G among the groups was found to be barely significant using ANOVA, but was not substantial enough to discern significance between any two pairs of groups.

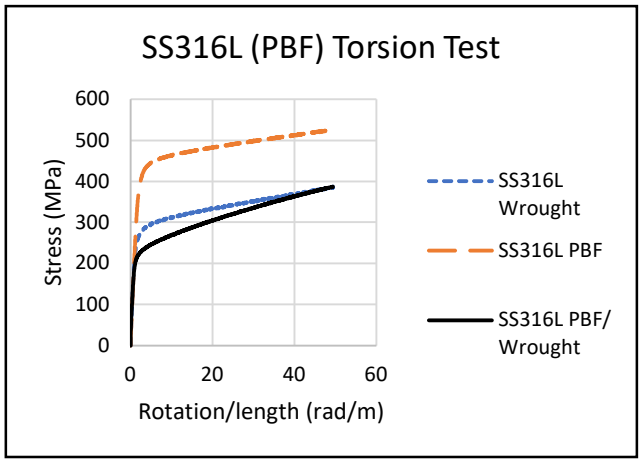

Figure 6. Average torsion test stress/rotation.

Table 4. Measured torsion properties.

		Wrought	PBF	PBF/Wrought
τ_y	Mean	220 MPa	380 MPa	200 MPa
	StdDev	17 MPa	4.6 MPa	22 MPa
G	Mean	71 GPa	70 GPa	61 GPa
	StdDev	3.7 GPa	0.4 GPa	5.5 GPa

Preprints (www.preprints.org) | NOT PEER-REVIEWED | Posted: 12 April 2021 doi:10.20944/preprints202104.0314.v1

Table 5. Statistical analysis of torsion samples.

	Comparison	Statistical test (α=0.05)	Different? (p ≤ 5.0E-2)
τ_y	Among group	ANOVA	**Yes** (p = 7.3E-5)
	Wrought vs PBF	t-test (equal variance)	**Yes** (p = 4.7E-4)
	Wrought vs PBF/Wrought	t-test (equal variance)	**No** (p = 4.3E-1)
	PBF vs PBF/Wrought	t-test (equal variance)	**Yes** (p = 5.0E-3)
G	Among group	ANOVA	**Yes** (p = 4.9E-2)
	Wrought vs PBF	t-test (uneq. variance)	**No** (p = 7.4E-1)
	Wrought vs PBF/Wrought	t-test (equal variance)	**No** (p = 1.1E-1)
	PBF vs PBF/Wrought	t-test (uneq. variance)	**No** (p = 1.0E-1)

3.3. Microscopy

Microscopy was done to examine the interface between the PBF and wrought 316L, while also allowing for characterization of grain size. Figure 7 shows a representative image of the interface of the PBF/wrought 316L specimen. Formal analysis of void content was not done, but the micrograph in Figure 7 (at 63X magnification) does not show evidence of voids at the interface or in the PBF material.

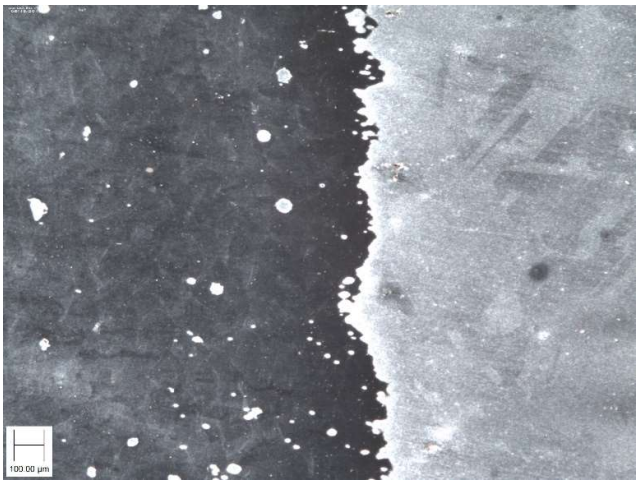

Figure 7. SS316L PBF/wrought interface (63X magnification).

EBSD scans were also done for the specimen, providing images of grain structure, and allowing for average grain size calculations. Grain maps for the wrought material and PBF material are shown in Figure 8.

Preprints (www.preprints.org) | NOT PEER-REVIEWED | Posted: 12 April 2021 doi:10.20944/preprints202104.0314.v1

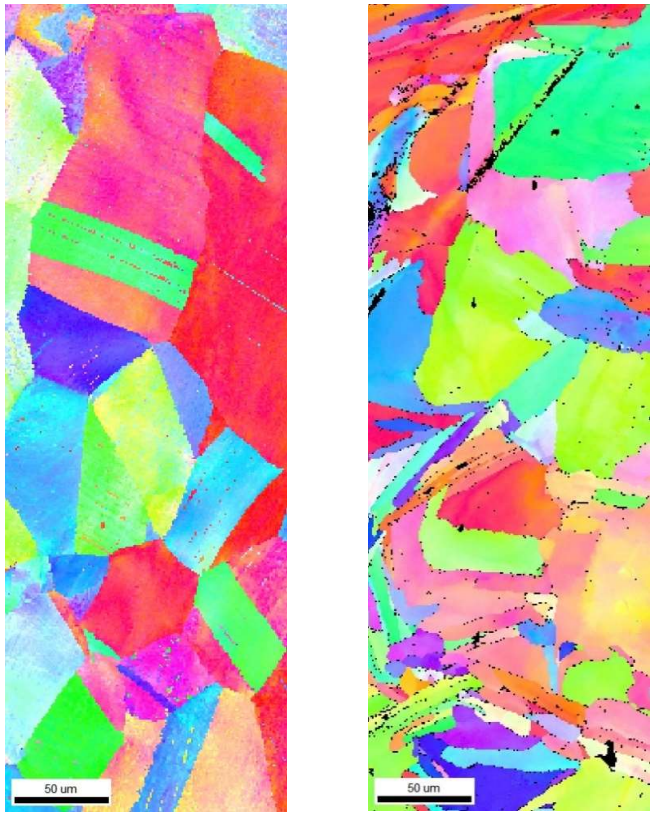

(a) (b)

Figure 8. EBSD grain maps of (a) wrought 316L with average grain size of 60 μm, and (b) PBF 316L with average grain size of 48 μm. Scans were taken about 10 mm away from the PBF/wrought interface.

4. Discussion

4.1 Analysis of Wrought and PBF AM Specimens

The tensile and torsion stress curves of the monolithic PBF AM material were higher than those of the wrought material. The measured tensile yield strength, ultimate tensile strength, and torsional yield strength of the PBF specimens were consistently greater than those of the wrought specimens, and plastic deformation occurred at higher stresses for given displacement levels. The PBF specimens also failed in tension at lower strain, showing less ductility than the wrought material. EBSD analysis of the wrought and PBF materials supports the test results. As seen in Figure 8, the SS316L wrought material had an average grain size of 60 μm, while the PBF material had an average grain size of 48 μm. Since SS316L exhibits a very strong Hall-Petch relationship, where yield stress increases with smaller grain size [9], the smaller grains in the PBF material increase its strength over the wrought material. Smaller grain size in the PBF material also contributes to the reduced ductility, as slip of the grains is more restricted.

4.2 Analysis of Hybrid PBF/Wrought Specimens

In all tensile tests, the PBF/wrought specimens consistently experienced failure well away from the interface between the two materials. This demonstrates good bond quality at the interface and strengthening of the weaker material by the stronger material near the interface. Because no failures occurred at the interface, the actual interfacial strength could not be determined, other than the conclusion that it would be higher than the observed stresses at failure. As mentioned above, the PBF

material exhibited significantly higher strength than the wrought material, most likely due to its reduced grain size. In the hybrid PBF/wrought specimens, plastic deformation and final tensile failure consistently occurred almost exclusively within the lower strength wrought portions of the specimens. The measured tensile yield strength, ultimate tensile strength, and torsional yield strength of the PBF/wrought specimens were not significantly different from the baseline wrought specimens, supporting this observation.

5. Conclusions

Powder bed fusion (PBF) AM 316L stainless steel material was built up on existing wrought 316L blocks, allowing for characterization of bond strength in both uniaxial tension and torsion. The following conclusions were drawn from the experimental results:

1. Hybrid PBF/wrought tensile failures occurred well away from the bond interface, in the wrought portion of the specimen, demonstrating that interface bond quality was good. Torsion specimens also showed concentrated deformation in the wrought portion of each specimen.
2. The yield and ultimate tensile strengths of the 316L PBF material was significantly greater than that of the wrought material of the same alloy.
3. Average grain sizes for the 316L PBF material were 48 μm versus 60 μm for the wrought material. The Hall-Petch effect, which is pronounced in 316L, is likely the reason for the greater strength of the PBF material and explains the behavior of the hybrid PBF/wrought specimens in uniaxial tension and torsion.

Acknowledgements: The authors would like to thank Robert Smith, of Qualified Rapid Products, and Jason Jones, of Hybrid Manufacturing Technologies, for fabricating the test specimens and providing insight into the specimen design.

Author Contributions: Conceptualization, John R. Linn, Michael P. Miles, and Jason M. Weaver; methodology, Jason M. Weaver, Michael P. Miles, and John R. Linn; testing, John R. Linn.; validation, Jason M. Weaver and Michael P. Miles; formal analysis, John R. Linn, Jason M. Weaver, and Michael P. Miles; writing—original draft preparation, John R. Linn; writing—review and editing, Jason M. Weaver and Michael P. Miles; visualization, Jason M. Weaver; project administration, Jason M. Weaver. All authors have read and agreed to the published version of the manuscript.

Funding: This research received no external funding.

Conflicts of Interest: The authors declare no conflict of interest.

References

1. Frazier, W.E., *Metal Additive Manufacturing: A Review.* Journal of Materials Engineering and Performance, 2014. **23**(6): p. 1917-1928 DOI: 10.1007/s11665-014-0958-z.
2. Everton, S.K., et al., *Review of In-Situ Process Monitoring and In-Situ Metrology for Metal Additive Manufacturing.* Materials & Design, 2016. **95**: p. 431-445 DOI: 10.1016/j.matdes.2016.01.099.
3. Mandil, G., V.T. Le, and H. Paris, *Building New Entities from Existing Titanium Part by Electron Beam Melting: Microstructures and Mechanical Properties.* International Journal of Advanced Manufacturing Technology, 2016. **85**: p. 1835-1846 DOI: 10.1007/s00170-015-8049-3.
4. Zhao, G., et al., *Nonplanar slicing and path generation methods for robotic additive manufacturing.* The International Journal of Advanced Manufacturing Technology, 2018. **96**(9-12): p. 3149-3159.
5. Gibson, I., D. Rosen, and B. Stucker, *Powder Bed Fusion Processes*, in *Additive Manufacturing Technologies*. 2015, Springer: New York DOI: 10.1007/978-1-4939-2113-3_5.
6. Jones, J., *Repurposing mainstream CNC machine tools for laser-based additive manufacturing*. SPIE LASE. Vol. 9738. 2016: SPIE.

7. Jones, J., et al. *Remanufacture of turbine blades by laser cladding, machining and in-process scanning in a single machine*. in *23rd Annual International Solid Freeform Fabrication Symposium*. 2012. Austin.
8. *ASTM E8 / E8M-16ae1, Standard Test Methods for Tension Testing of Metallic Materials*. 2016, ASTM International: West Conshohocken DOI: 10.1520/E0008_E0008M-16AE01.
9. Qin, W., et al., *Effects of grain size on tensile property and fracture morphology of 316L stainless steel.* Materials Letters, 2019. **254**: p. 116-119.